Adaptor protein mediates dynamic pump assembly for bacterial metal efflux

Ace George Santiago[a,1], Tai-Yen Chen[b,1], Lauren A. Genova[a], Won Jung[a], Alayna M. George Thompson[c], Megan M. McEvoy[d,e], and Peng Chen[a,2]

[a]Department of Chemistry and Chemical Biology, Cornell University, Ithaca, NY 14853; [b]Department of Chemistry, University of Houston, Houston, TX 77204; [c]Department of Chemistry and Biochemistry, University of Arizona, Tucson, AZ 85721; [d]Department of Microbiology, Immunology and Molecular Genetics, University of California, Los Angeles, CA 90095; and [e]Molecular Biology Institute, University of California, Los Angeles, CA 90095

Edited by Edward I. Solomon, Stanford University, Stanford, CA, and approved May 16, 2017 (received for review March 21, 2017)

Multicomponent efflux complexes constitute a primary mechanism for Gram-negative bacteria to expel toxic molecules for survival. As these complexes traverse the periplasm and link inner and outer membranes, it remains unclear how they operate efficiently without compromising periplasmic plasticity. Combining single-molecule superresolution imaging and genetic engineering, we study in living *Escherichia coli* cells the tripartite efflux complex CusCBA of the resistance–nodulation–division family that is essential for bacterial resistance to drugs and toxic metals. We find that CusCBA complexes are dynamic structures and shift toward the assembled form in response to metal stress. Unexpectedly, the periplasmic adaptor protein CusB is a key metal-sensing element that drives the assembly of the efflux complex ahead of the transcription activation of the *cus* operon for defending against metals. This adaptor protein-mediated dynamic pump assembly allows the bacterial cell for efficient efflux upon cellular demand while still maintaining periplasmic plasticity; this could be broadly relevant to other multicomponent efflux systems.

multicomponent efflux complex | substrate-responsive dynamic assembly | periplasmic adaptor protein | metal sensing | single-molecule tracking

Bacteria are often exposed to harsh environments, including high metal ion concentrations and toxic organic molecules. Efflux of metal ions helps bacteria maintain appropriate intracellular concentrations of essential metals while removing toxic ones (1–6). Efflux of organic molecules, including antibiotics, is a key mechanism for bacterial multidrug resistance (7–14). The tripartite resistance–nodulation–division (RND) family efflux pumps confer major clinically relevant drug resistance in Gram-negative bacteria such as *Escherichia coli* and the infectious *Pseudomonas aeruginosa* (7–14). They are composed of a proton-motive-force–driven inner-membrane pump, a periplasmic adaptor protein, and an outer-membrane channel. Once assembled, these pumps traverse the cell periplasm, providing a direct extrusion pathway from the periplasm (and cytoplasm) to the outside of the cell. However, these direct pathways also tightly link the inner and outer membranes, which, if overly stable, would impede the periplasm's plasticity and ability to respond dynamically to external and internal stimuli to buffer the cell from changes in its surroundings (15).

How can tripartite efflux pumps operate without compromising the dynamic nature of the periplasm? One possibility is that these efflux complexes are dynamic structures and assemble only in the presence of their substrates. This mechanism has been hypothesized for the *E. coli* HlyBD–TolC complex (16), in which HlyB is a ATP-binding cassette superfamily efflux pump. However, experimental validation of this mechanism, as well as its relevance to the RND family efflux pumps, remains elusive, partly due to the difficulty in studying two membrane proteins together with a periplasmic protein under physiologically relevant conditions.

A recent imaging study (17) showed that AcrB, an RND family drug efflux inner-membrane pump that can form a complex with adaptor protein AcrA and channel protein TolC, could potentially exchange with another inner-membrane pump AcrD. This exchange is inhibited by substrate molecules, suggesting a substrate-responsive dynamic AcrBA–TolC complex. It is unclear, however, whether this complex is dynamic on its own or merely appears so because of the competing pump AcrD that shares the same adaptor and channel proteins. Moreover, the substrate-responding component of this system remains unknown, and both membrane pumps, AcrB and AcrD, are potential candidates because of their substrate-binding capabilities.

Here, using superresolution single-molecule tracking (SMT) via stroboscopic imaging (18, 19), we probe the dynamic assembly of a tripartite RND family efflux complex CusCBA in living *E. coli* cells, circumventing the purification of membrane proteins required for in vitro experiments. This CusCBA complex is encoded in the chromosomal *cusCFBA* operon, which, along with the two-component *cusRS* regulator–sensor, constitutes *E. coli*'s *cus* system for defending against toxic Cu^+ and Ag^+ ions (2, 20). CusA is a trimeric inner-membrane pump of the heavy-metal efflux subfamily and has multiple metal-binding sites (21). CusB is a periplasmic adaptor protein, which on its own is a monomer and can bind Cu^+ and Ag^+ strongly (22). CusC is a trimeric outer-membrane channel (23) and does not bind metal. Together, these proteins form the tripartite $CusC_3B_6A_3$ complex that extrudes Cu^+ and Ag^+ ions (21, 23–25). By resolving and quantifying the populations of different

Significance

Multicomponent efflux pumps confer clinically relevant drug resistance in Gram-negative bacteria. These pumps, once assembled to function, traverse the periplasm linking inner and outer membranes tightly. However, little is known on how these pumps can operate efficiently without compromising periplasmic plasticity. We show here that in *Escherichia coli*, the tripartite complex CusCBA for Cu^+ and Ag^+ efflux exists as a dynamic structure and shifts toward the assembled form in response to metal stress. Unexpectedly, the periplasmic adaptor protein CusB is a key metal-sensing protein that mediates the complex assembly. This adaptor protein-mediated dynamic pump assembly allows the bacterial cell for efficient efflux on cellular demand while still maintaining periplasmic plasticity; it can be broadly relevant to other multicomponent efflux systems.

Author contributions: A.G.S., T.-Y.C., and P.C. designed experiments; A.G.S., T.-Y.C., L.A.G., and W.J. performed experiments; A.M.G.T. and M.M.M. contributed to experiments; W.J. contributed to data analysis; A.G.S., T.-Y.C., and P.C. analyzed data; and A.G.S., T.-Y.C., and P.C. wrote the paper.

The authors declare no conflict of interest.

This article is a PNAS Direct Submission.

[1]A.G.S. and T.-Y.C. contributed equally to this work.

[2]To whom correspondence should be addressed. Email: pc252@cornell.edu.

This article contains supporting information online at www.pnas.org/lookup/suppl/doi:10.1073/pnas.1704729114/-/DCSupplemental.

diffusive behaviors of single CusA molecules in combination with genetic manipulations of the cell, we find that CusCBA complexes on their own exist in a dynamic exchange between the disassembled and assembled states in the cell under both substrate-depleted and substrate-stressed conditions. In response to metal stress, CusA shifts toward the assembled state through a synergistic increase in association kinetics and decrease in dissociation kinetics of the CusCBA complex. Unexpectedly, the periplasmic adaptor protein CusB is a key metal-responsive protein, whose metal binding allosterically mediates the assembly of the CusCBA complex. Moreover, CusB appears to be the first responder in sensing metal for assembling CusCBA for efflux, earlier than transcription activation of the *cus* operon. This adaptor protein-mediated pump assembly allows the bacterial cell to expel toxic chemicals efficiently upon cellular demand while still maintaining periplasmic plasticity, and is likely broadly relevant to other types of multicomponent efflux systems.

Results and Analysis

Two Diffusion States of CusA Shift in Relative Population Under Metal Stress. To visualize and examine the assembly dynamics of CusCBA in a living *E. coli* cell, we chose to tag CusA at its C terminus with the photoconvertible fluorescent protein mEos3.2 (26, 27) at its chromosomal locus [i.e., CusA^{mE}, referred to as the wild-type (WT) cell; *SI Appendix*, section 1.1]. The C terminus of CusA is exposed to the cytosol (21), whereas for CusB and CusC, being periplasmic and outer membrane proteins, respectively, makes it problematic for the folding and maturation of fluorescent protein tags (28). Cell growth assays and protein gel analyses show that CusA^{mE} is functional, and the mE tag is not cleaved in the cell (*SI Appendix*, Figs. S3 and S4*A*). Photoactivation localization microscopy (PALM) (29–31) and confocal fluorescence microscopy confirm that CusA^{mE} is membrane localized (*SI Appendix*, Fig. S5). Oligomerization analysis of the imaging results from PALM also supports that CusA^{mE} molecules are expectedly stable trimers (21, 24) in the cell (*SI Appendix*, section 5).

Using time-lapse stroboscopic imaging (18, 19) (4-ms laser exposure; 60-ms lapse), we tracked the motions of single photoconverted CusA^{mE} proteins in a cell at tens of nanometer precision until their mE tags photobleached (Fig. 1*A*). This stroboscopic imaging approach allows us to image diffusive proteins with effective diffusion constants up to ~3.7 $\mu m^2 \cdot s^{-1}$, sufficient even for small proteins freely diffusing in the cytosol with effective diffusion constants of typically ~3–4 $\mu m^2 \cdot s^{-1}$ (19). Cells are viable under our imaging conditions (*SI Appendix*, Fig. S7). From this single-molecule tracking, we obtained the probability distribution function (PDF) of the displacement length r per time lapse for single CusA^{mE} proteins. This PDF(r), although containing rich information on the diffusive behaviors of CusA^{mE}, is skewed because of the confinement effect from the 2D projection of diffusion on the curved *E. coli* membrane surface (32). We thus applied an inverse transformation of confined displacement distribution (ITCDD) (32, 33) to deconvolute out this confinement effect, so as to extract reliably the minimal number of diffusion states, as well as their intrinsic diffusion constants and fractional populations (Fig. 1*B* and *SI Appendix*, section 8).

We first examined CusA^{mE} in WT cells grown in a copper-depleted medium. The ITCDD-corrected PDF(r) is sufficiently fitted by two diffusion states (Fig. 1*B* and *SI Appendix*, section 8). The slower diffusion state has a diffusion constant $D_s = 0.052 \pm 0.011$ $\mu m^2 \cdot s^{-1}$, which is almost stationary with our localization precision (~20 nm), and a fractional population $A_s = 55 \pm 6\%$; the faster state has $D_f = 0.27 \pm 0.06$ $\mu m^2 \cdot s^{-1}$ and $A_f = 45 \pm 6\%$ (Fig. 1*C*).

We then examined CusA^{mE} in WT cells stressed for 30 min under 500 μM Cu^{2+}, which is known to cause maximal transcription induction of the *cusCFBA* operon in the cell (20). The same two diffusion states are resolved. However, their fractional populations have shifted significantly toward the slow state with $A_s = 91 \pm 6\%$ (Fig. 1*C*), even though the cellular CusA^{mE} concentration shows no significant change (0.13 ± 0.11 μM) under copper stress (Fig. 1*D*).

Metal-Responsive Dynamic CusCBA Pump Assembly. We assigned the faster diffusion state of CusA^{mE} to be dominated by free CusA

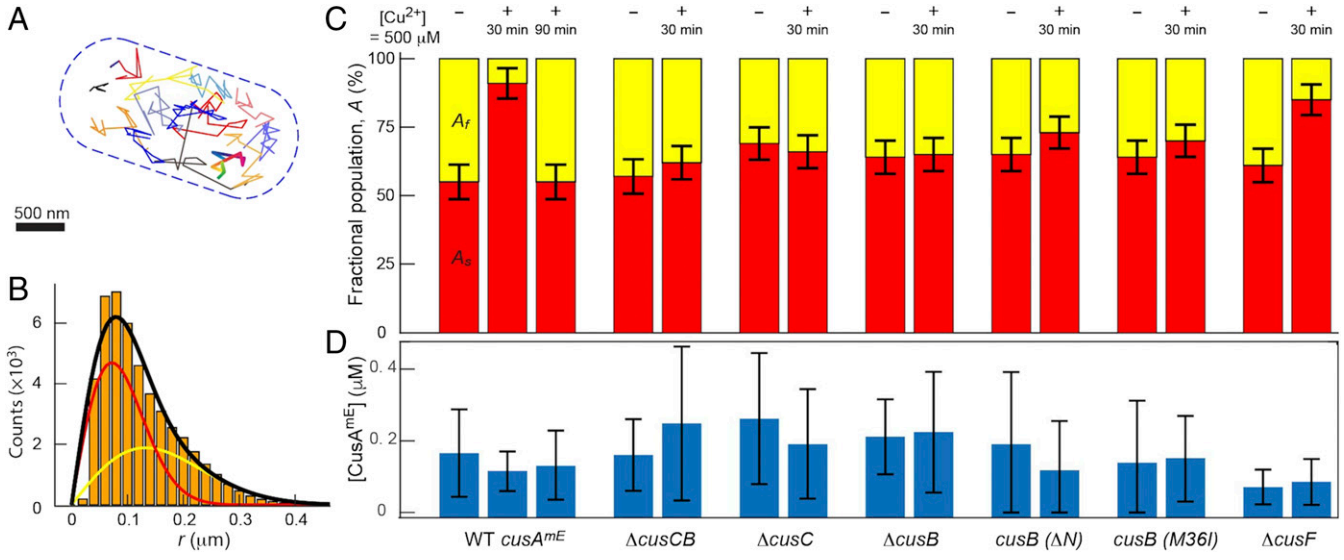

Fig. 1. SMT reveals dynamic population shifts between two different CusA^{mE} diffusion states. (*A*) Overlay of many position trajectories of single CusA^{mE} proteins in a living WT *E. coli* cell. The blue dashed line is the cell boundary. (*B*) ITCDD-corrected histogram of displacement length r per time lapse (60 ms) of CusA^{mE} from a total of 8,354 molecules and ~350 WT cells grown in a copper-depleted medium. Solid lines represent the overall PDF (black, *SI Appendix*, Eq. **S2**) and the resolved fast (yellow) and slow (red) diffusion states, all multiplied by a scaling factor to account for the actual number of measured displacements. (*C* and *D*) Fractional populations of the fast (A_f, yellow) and slow (A_s, red) diffusion states (*C*), and cellular concentrations (*D*, in terms of CusA trimers), of CusA^{mE} in various strains, grown in a copper-depleted medium (–) or stressed with [Cu^{2+}] of 500 μM for 30 and 90 min. All error bars are SD.

trimers that are not assembled into CusCBA complexes and that might even have a few CusB protein molecules attached (Fig. 2*A*, *Left*). This attribution comes from the following reasoning. First, its diffusion constant ($D_f \sim 0.27\ \mu m^2 \cdot s^{-1}$) is consistent with those reported for simple inner-membrane proteins (0.18–0.52 $\mu m^2 \cdot s^{-1}$) (34–36). Second, the interaction affinity of CusA and CusB in their apo forms is in the micromolar range (24); with cellular CusA protein concentration in the submicromolar range (Fig. 1*D*), some disassembly of the CusCBA complex is likely, especially when cells are grown in copper-depleted media.

We assigned the slower diffusion, almost stationary, state ($D_s \sim 0.052\ \mu m^2 \cdot s^{-1}$) of CusA^{mE} to contain a significant contribution from the fully assembled CusCBA complex (i.e., $CusC_3B_6A_3$; Fig. 2*A*, *Right*). This CusCBA complex is expected to not diffuse much and be almost stationary because it traverses the periplasm (and the peptidoglycan layer), directly linking the inner and outer membranes. This slower diffusion state of CusA^{mE} might also have contributions from CusA trimers clustered together within the inner membrane, as it is known that membrane protein clustering can slow their motions significantly (37). Moreover, the distribution of pairwise distances between the tracked CusA^{mE} molecules shows a peak at a shorter distance than that from a simulation of randomly distributed CusA trimers in the membrane, supporting some level of clustering of CusA^{mE} in the cell (Fig. 3*A*, blue vs. black lines).

We further attributed the population shift toward the slower diffusion state under copper stress to an increased population of the CusCBA complex (Fig. 2*A*) (rather than increased CusA clustering, as no shortening of the pairwise distances was observed; Fig. 3*A*, blue vs. green lines). This shift would thus reflect a metal-responsive dynamic CusCBA assembly that would allow the cell for more effective metal efflux.

To validate our assignments, we examined CusA^{mE} in a *cusC* and *cusB* double-deletion strain (i.e., Δ*cusCB*) where no CusCBA complexes can exist. Surprisingly, SMT still resolves the two diffusion states in this strain grown in the copper-depleted medium, where the fractional population A_s of the slower state is comparable to that in the WT strain (Fig. 1*C*). We postulated that the slower diffusion state here must come from significant CusA trimer clustering in the membrane (*SI Appendix*, Fig. S13*A*). Consistent with our postulate, pairwise distance distribution of tracked CusA^{mE} molecules in this Δ*cusCB* strain shows significant shortening compared with that in the WT strain (Fig. 3 *A* and *C*). Past studies have shown that membrane protein clustering is often correlated with their spatial segregation toward the two poles of an *E. coli* cell, possibly because larger membrane curvature restricts cluster escaping (38). We therefore examined the localization distribution of CusA^{mE} in this Δ*cusCB* strain: compared with that of the WT strain and the simulated random distribution, a

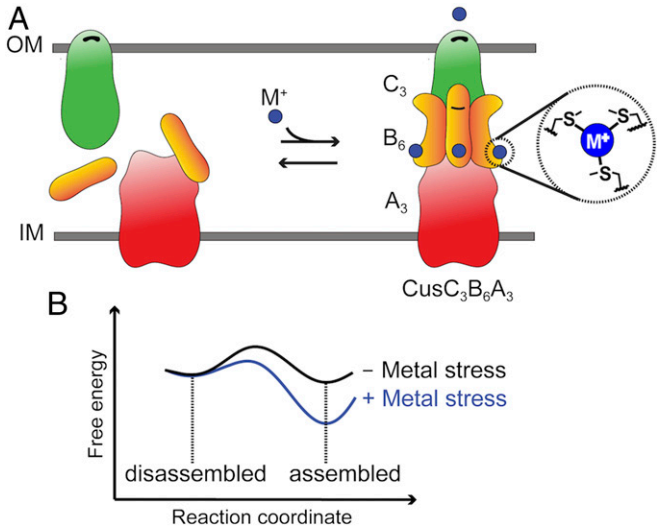

Fig. 2. Adaptor protein-mediated metal-responsive dynamic assembly–disassembly model of CusCBA complex. (*A*) In the absence of the metal substrate (Cu^+ or Ag^+), CusCBA is dominantly disassembled (*Left*). Upon binding the metal substrate (i.e., M^+) at its trimethionine site, CusB changes conformation and shifts the equilibrium toward the fully assembled $CusC_3B_6A_3$ complex for efflux (*Right*). IM, inner membrane; OM, outer membrane. (*B*) Schematic potential energy surface of the metal-responsive dynamic assembly shift of CusCBA, where the changes in energy barriers reflect the changes of the assembly and disassembly rates.

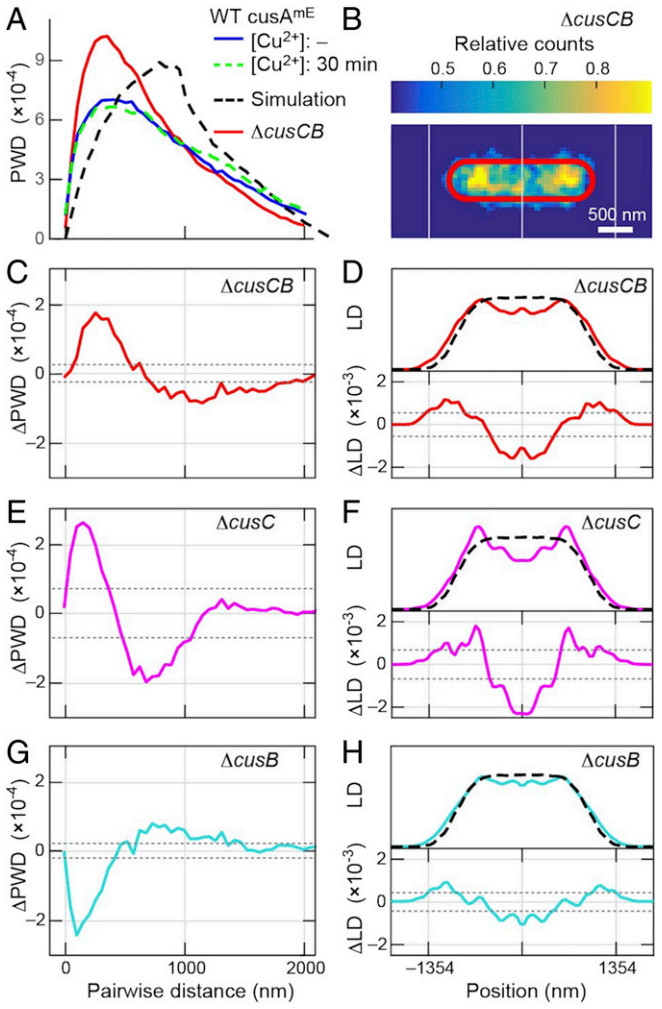

Fig. 3. Pairwise distance distribution and localization distribution for identifying clustering and bipolar accumulation of CusA. (*A*) Normalized pairwise distance distribution (PWD) of tracked CusA^{mE} molecules in WT strain (without and with 30-min copper stress) and Δ*cusCB* strain without copper stress, as well as from a simulation of random localizations. (*B*) Two-dimensional distribution of all CusA^{mE} initial localizations in the Δ*cusCB* strain (8^2-nm^2 bin size) without copper stress. Histogram normalized to the maximum count and overlaid on the average cell boundary (red solid line). (*C*) Difference of normalized PWD (ΔPWD) of Δ*cusCB* from that of WT strain without copper stress in *A*. Gray dotted lines: 99.7% confidence bounds. (*D*, *Top*) One-dimensional normalized localization distribution (LD) by projecting *B* onto the long axis of the cell (red line) and that from the simulation of random localizations (black dashed line). (*D*, *Bottom*) Difference between data and simulation (ΔLD, red line) and the 99.7% confidence bounds (gray dotted lines). (*E*–*H*) Same as *C* and *D*, but for the Δ*cusC* and Δ*cusB* strains.

bipolar accumulation of CusA^{mE} is clearly observable (Fig. 3 *B* and *D*), further supporting our CusA clustering postulate in this Δ*cusCB* strain.

We further examined this Δ*cusCB* double-deletion strain after 30-min copper stress. The significant CusA trimer clustering persists, as reflected by the shortened pairwise distance distribution and bipolar accumulation of CusA^{mE} (*SI Appendix*, Figs. S10*B* and S12*B*). However, no population shift is observable toward the slower diffusion state of CusA^{mE} (Fig. 1*C*), indicating that copper stress does not induce significant changes in CusA trimer clustering. More important, the lack of a copper-induced population shift here indicates that the metal-induced CusCBA assembly in the WT strain requires the presence of CusB, CusC, or both, and is not a result of changes in the extent of CusA trimer clustering.

Adaptor Protein CusB Is a Key Responsive Protein. To identify whether CusC or CusB is a key player for the metal-responsive assembly of CusA into the CusCBA complex, we examined the single-deletion Δ*cusC* and Δ*cusB* strains. Relative to the double-deletion Δ*cusCB* strain, these two strains are equivalent to back-introducing the CusB or CusC protein into the cell individually. For both of these single-deletion strains grown in the copper-depleted medium, SMT of CusA^{mE} still resolves the two diffusion states with their respective fractional populations comparable to those in the Δ*cusCB* strain (Fig. 1*C*). For the Δ*cusC* strain, the slow diffusion state must still be dominated by CusA trimer clustering (*SI Appendix*, Fig. S13*B*) because the shortened pairwise distance distribution and the accompanying bipolar accumulation of CusA^{mE} are still apparent (Fig. 3 *E* and *F*).

The similarities between the Δ*cusC* and Δ*cusCB* strains therefore indicate that, once CusC is deleted, CusA will significantly cluster and accumulate toward the poles of the cell, in which CusB does not play significant roles even though CusB may interact with one or both of the diffusion components of CusA. The changes in CusA's clustering could come from the lack of interaction with CusC increasing CusA trimer's affinity toward itself, resulting in more CusA trimer clustering and concurrent accumulation toward the poles. Consistently, no copper-induced population shift was observed between the diffusion states in the Δ*cusC* strain (Fig. 1*C*), as in the Δ*cusCB* strain, both of which reflect that CusA trimer clustering has no significant dependence on copper stress.

In contrast, for the Δ*cusB* strain, the shortened pairwise distance distribution and bipolar accumulation of CusA^{mE} have either vanished or diminished significantly compared with the Δ*cusCB* strain (Fig. 3 *G* and *H* vs. *C* and *D*). Thus, the slower diffusion state here must not be dominated by CusA trimer clustering. Past biochemical studies (7) have shown that, for the RND family drug efflux complex AcrBA–TolC, the inner-membrane pump AcrB can directly interact with the outer-membrane channel protein TolC in the absence of the adaptor protein AcrA (39, 40). A protein docking model (24) also showed that CusA can interact with CusC directly. We therefore attributed the slower state in this Δ*cusB* strain to have a significant contribution from the assembled bicomponent CusCA complex (*SI Appendix*, Fig. S13*C*), whose diffusive behavior should be similar to that of the CusCBA complex, as it also traverses the periplasm and connects the inner and outer membranes (although it is likely nonfunctional for copper or silver efflux). Importantly, copper stress does not cause a population shift from the faster (free CusA) to the slower (CusCA complex) state in this Δ*cusB* strain (Fig. 1*C*), in contrast to the WT strain, in which the slower state has a significant contribution from the CusCBA complex. Therefore, CusB is a key protein for the metal-induced assembly of the CusCBA complex, whereas CusC, although being an essential component of CusCBA assembly and able to interact directly with CusA in the absence of CusB, does not contribute to the metal response in shifting CusCBA toward the assembled state.

Molecular and Kinetic Basis of CusB's Metal Sensing in Shifting CusCBA Assembly. A likely molecular component of CusB in mediating the metal-responsive assembly of the CusCBA complex is its trimethionine site (i.e., M21, M36, and M38), which can bind Cu^+ and Ag^+ under physiological conditions and undergo metal transfer with the metallochaperone CusF, which is also part of the *cusCFBA* operon (41–43). To test this, we made a *cusB*(ΔN) strain, in which CusB's N-terminal residues 1–61 containing this site were truncated (42); the signal peptide sequence was maintained so as to not affect its targeting to the periplasm. In addition to resolving the faster diffusion state, SMT of CusA^{mE} in this *cusB*(ΔN) strain still reveals the slower diffusion state, with a fractional population comparable to that in the WT strain (Fig. 1*C*). More important, this truncation abolishes the copper-induced population shift toward the slower state (Fig. 1*C*), whereas pairwise distance distribution and localization distribution analyses show no increase in CusA clustering and no bipolar accumulation under copper-depleted or copper-stressed conditions (*SI Appendix*, Figs. S10*E* and S12*E*). These results suggest that CusB's N-terminal domain, and thus its trimethionine metal-binding site, is essential for its ability to mediate the metal-responsive assembly of the CusCBA complex.

To further probe the role of CusB's trimethionine metal-binding site, we created a *cusB*(M36I) strain in which one of the metal-binding methionine (Met36) was mutated to isoleucine to abolish CusB's specific binding of copper or silver (22, 43). Pairwise distance distribution and localization distribution analyses show a slight increase in CusA clustering and its bipolar accumulation (*SI Appendix*, Figs. S10*F* and S12*F*), which is also reflected by the slight increase of the slow state population compared with the WT strain (Fig. 1*C*). More important, this mutation abolishes the copper-induced population shift toward the slow state, further supporting that metal binding to CusB's trimethionine site is essential for the metal-responsive assembly of the CusCBA complex in the cell.

Past studies have shown that CusB can obtain copper and silver from the periplasmic metallochaperone CusF through direct protein–protein interactions (41–43). To probe whether CusF is involved with CusB in mediating the metal-responsive CusCBA assembly, we further studied CusA^{mE} in a Δ*cusF* strain. Under copper-depleted conditions, SMT of CusA^{mE} still resolves the slower and faster diffusion states, with fractional populations comparable to those in the WT strain (Fig. 1*C*). Pairwise distance distribution and localization distribution analyses show neither an increase in CusA clustering nor a bipolar accumulation in this Δ*cusF* strain (*SI Appendix*, Figs. S10*G* and S12*G*). Moreover, under copper stress, a clear population shift is observable toward the slower diffusion state, comparable in magnitude to that of the WT strain (Fig. 1*C*). Therefore, CusF does not play a significant role in CusB's ability to bind metal and mediate the dynamic assembly of CusCBA, and CusB can sense and bind metal directly in the periplasm.

To probe the kinetic basis of CusB-mediated metal-responsive CusCBA assembly, we further analyzed the displacement-vs.-time trajectories of single CusA^{mE} in the WT strain (*SI Appendix*, Fig. S14), obtainable from the tracking trajectories as in Fig. 1*A*. Thresholding this displacement trajectory with an upper displacement limit selects out those small displacements and gives the estimate of the individual time durations (i.e., the microscopic residence time τ) of a single CusA^{mE} within an assembled CusCBA complex. Using a two-state kinetic model comprising the disassembled and assembled CusA, as well as correcting for the photobleaching/blinking kinetics of the mE tag, we could analyze the distribution of τ to obtain k_d, the apparent first-order disassembly rate constant of the CusCBA

complex (*SI Appendix*, section 11.1 and Fig. S14 *B–D*). Assuming a quasiequilibrium between the two states further allowed us to use their fractional populations to derive k_a, the pseudo–first-order assembly rate constant (*SI Appendix*, section 11.1). Using simulations of two-state membrane diffusions, we further validated the reliability of our analysis in obtaining kinetic trends (*SI Appendix*, section 11.2).

The disassembly and assembly rate constants are on the order of 10^0 to 10^1 s^{-1}, corresponding to subsecond timescales (Fig. 4). In the WT strain, the disassembly rate constant decreases while the assembly rate constant increases with 30-min copper stress (Fig. 4*A*). Similar trends are clear in the Δ*cusF* strain, but the values of the rate constants are slightly larger (Fig. 4*B*). Therefore, when CusB binds metal, it not only increases the assembly kinetics but also decreases the disassembly kinetics of the CusCBA complex, possibly via altering the potential energy surfaces of complex assembly and synergistically resulting in a dynamic population shift toward the assembled state (Fig. 2*B*). CusF here, although not significantly affecting the thermodynamics of the population shift, could facilitate the kinetics underlying the assembly. It is worth noting that we only analyzed the kinetics in the WT *cusA*^{mE} and Δ*cusF* strains, where the slow diffusion state is dominated by the assembled CusCBA complex and CusA trimer clustering is insignificant. Nevertheless, the kinetics of assembly–disassembly here has some contamination from clustering–unclustering kinetics. However, the change in kinetics upon Cu stress here is reliable because CusA clustering is independent of Cu stress.

Discussion

We have quantified the diffusive behaviors of individual CusA^{mE} in living *E. coli* cells in combination with genetic manipulations. We have discovered that in the absence of metal stress (when efflux is not needed), the inner-membrane pump CusA of the CusCBA complex has a significant population in the disassembled state in the cell, allowing for periplasmic plasticity. Under metal stress, the periplasmic adaptor protein CusB acts as a metal sensor, shifting CusA's dynamic assembly toward the complete CusCBA complex for metal efflux. This shift is associated with an increase in the assembly kinetics and a concurrent decrease in the disassembly kinetics, both at subsecond timescales. The metal sensing by CusB results from metal binding to its trimethionine site, which is known to induce large conformational changes in its N-terminal domain (22), thus providing an allosteric mechanism for its sensing role. This CusB-mediated dynamic assembly of the CusCBA complex would also provide a molecular mechanism for an earlier in vitro observation that holo-CusB can activate CusA for metal efflux (44).

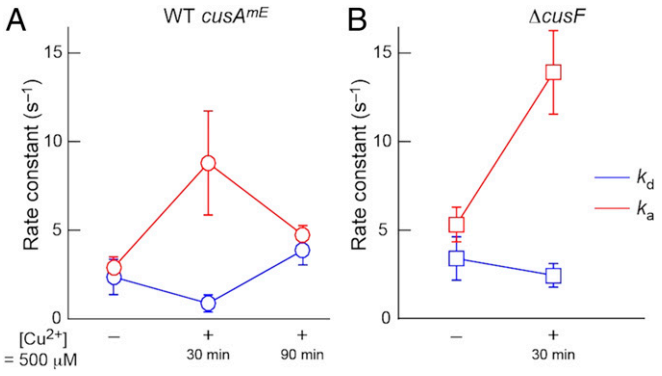

Fig. 4. Disassembly and assembly kinetics of CusCBA complex. Copper stress dependence of the apparent assembly (k_a) and disassembly rate constants (k_d) for the WT *cusA*^{mE} (*A*) and Δ*cusF* strains (*B*).

The metal-binding affinity of CusB is in the nanomolar range (22, 41) (*SI Appendix*, Table S6), significantly stronger than the micromolar metal-binding affinity of CusA (45). CusF, although having a metal-binding affinity comparable to CusB (46, 47), is not essential for CusCBA assembly, as we showed (Fig. 1*C*). The outer-membrane channel CusC cannot bind metal (it can interact directly with CusA to assemble, but the bicomponent CusCA assembly is not sensitive to metal stress). These relative metal-binding affinities suggest that CusB would be the first among the CusCBA proteins to acquire Cu^+ or Ag^+ upon metal level increase (either directly from surrounding solution or via the metallochaperone CusF in parallel); CusB hence is the first responder in the *cusCFBA* operon in sensing metal in the periplasm to shift the existing disassembled CusCBA proteins toward assembly within seconds for metal efflux. Once assembled, the metallated CusB could physically bridge CusA and CusC, and might also transfer the metal to CusA (44), for the eventual metal efflux function.

Moreover, CusS, the inner-membrane protein of the two-component CusRS regulatory system that senses periplasmic Cu^+ or Ag^+ to activate *cusCFBA* transcription, has a metal affinity of a few micromolar or weaker (48) (*SI Appendix*, Table S6), much weaker than that of CusB. Therefore, the transcription activation of the *cus* operon would not occur until the periplasmic metal concentration reaches the micromolar level, three orders of magnitude higher than the nanomolar affinity of CusB's metal binding. Consequently, metal binding by CusB would trigger the dynamic assembly of the basal level CusCBA proteins for metal defense, ahead of transcription activation of the *cusCFBA* operon.

We further quantified the mRNA and protein levels in the WT strain after activating the *cusCFBA* operon using copper stress. The mRNA levels of *cusC*, *cusB*, and *cusF* all increase in the cell, and so do their protein levels (*SI Appendix*, Figs. S4 and S15). Nonetheless, the increased protein levels of these three genes should not contribute significantly to a larger extent of CusCBA assembly, as the *cusB*(ΔN) and *cusB*(M36I) strains do not show an increased population of the assembled CusCBA complex under copper stress (Fig. 1*C*), even though these two strains should have similar increases in protein levels of these three genes. Strikingly, although its mRNA level increases, the protein level of CusA^{mE} shows no significant increase even after 90 min (Fig. 1*D*), when the copper-induced CusCBA assembly and the associated changes in its assembly–disassembly kinetics have already dissipated (Figs. 1*C* and 4*A*). Therefore, the transcription activation of *cusA* under copper stress merely maintains the CusA protein level in the cell for metal efflux, perhaps by compensating for faster protein degradation or less protein translation. The increased CusB and CusF protein levels after transcription activation could contribute to scavenging the extra Cu^+ and Ag^+ ions in the cell and possibly to later stripping the metal from CusS to eventually deactivate the CusRS regulatory system and perhaps from CusB in the CusCBA complex for disassembly.

There are many tripartite efflux complexes in Gram-negative bacteria (1–4, 7–14) besides those in the RND family; they all need the adaptor proteins to assemble into functional efflux complexes (*SI Appendix*, section 14 and Table S7). For the MacAB–TolC complex of the ATP-binding cassette superfamily, the adaptor protein MacA can bind its substrate with high affinity (49). For the multidrug efflux complex EmrAB–TolC of the major facilitator superfamily, the adaptor protein EmrA can also bind drugs (50). The substrate-binding capabilities of these adaptor proteins make it possible for them to mediate the substrate-responsive dynamic assembly of multicomponent efflux complexes, giving rise to a likely general mechanism for bacterial efflux that balances between efflux function and periplasmic

plasticity. This mechanism might also provide opportunities for antibacterial treatments that inhibit efflux complex assembly.

Materials and Methods

Materials and methods are described in *SI Appendix*, section 1. These include strains construction, immunoblotting for probing the fusion protein ($CusA^{mE}$) intactness, growth assays for testing the fusion protein functionality, sample preparation for single-molecule imaging and tracking, single-cell protein quantification, PALM microscopy, confocal microscopy, RT-PCR, and data analysis.

ACKNOWLEDGMENTS. We acknowledge the Army Research Office (Grant 66998LS) and the NIH (Grants AI117295, GM109993, GM106420, GM079192, and 5T32GM008500) for funding, Cornell University Biotechnology Resource Center (New York State Stem Cell Science Program Grant CO29155 and NIH Grant S10OD018516) for access to the Zeiss LSM880 confocal microscope, and Y. Aye for access to immunoblot imaging instrument.

1. Mealman TD, Blackburn NJ, McEvoy MM (2012) Metal export by CusCFBA, the periplasmic Cu(I)/Ag(I) transport system of *Escherichia coli*. *Curr Top Membr* 69:163–196.
2. Franke S, Grass G, Rensing C, Nies DH (2003) Molecular analysis of the copper-transporting efflux system CusCFBA of *Escherichia coli*. *J Bacteriol* 185:3804–3812.
3. Moore CM, Helmann JD (2005) Metal ion homeostasis in *Bacillus subtilis*. *Curr Opin Microbiol* 8:188–195.
4. Delmar JA, Su CC, Yu EW (2013) Structural mechanisms of heavy-metal extrusion by the Cus efflux system. *Biometals* 26:593–607.
5. Argüello JM, Raimunda D, Padilla-Benavides T (2013) Mechanisms of copper homeostasis in bacteria. *Front Cell Infect Microbiol* 3:73.
6. Djoko KY, Xiao Z, Wedd AG (2008) Copper resistance in *E. coli*: The multicopper oxidase PcoA catalyzes oxidation of copper(I) in Cu(I)Cu(II)-PcoC. *ChemBioChem* 9: 1579–1582.
7. Zgurskaya HI, Nikaido H (2000) Multidrug resistance mechanisms: Drug efflux across two membranes. *Mol Microbiol* 37:219–225.
8. Blair JM, Piddock LJ (2009) Structure, function and inhibition of RND efflux pumps in gram-negative bacteria: An update. *Curr Opin Microbiol* 12:512–519.
9. Paulsen IT, Brown MH, Skurray RA (1996) Proton-dependent multidrug efflux systems. *Microbiol Rev* 60:575–608.
10. George AM (1996) Multidrug resistance in enteric and other gram-negative bacteria. *FEMS Microbiol Lett* 139:1–10.
11. Nikaido H, Pagès JM (2012) Broad-specificity efflux pumps and their role in multidrug resistance of Gram-negative bacteria. *FEMS Microbiol Rev* 36:340–363.
12. Poole K (2001) Multidrug resistance in Gram-negative bacteria. *Curr Opin Microbiol* 4:500–508.
13. Ramos JL, et al. (2002) Mechanisms of solvent tolerance in gram-negative bacteria. *Annu Rev Microbiol* 56:743–768.
14. Ruggerone P, Murakami S, Pos KM, Vargiu AV (2013) RND efflux pumps: Structural information translated into function and inhibition mechanisms. *Curr Top Med Chem* 13:3079–3100.
15. Koch AL (1998) The biophysics of the gram-negative periplasmic space. *Crit Rev Microbiol* 24:23–59.
16. Thanabalu T, Koronakis E, Hughes C, Koronakis V (1998) Substrate-induced assembly of a contiguous channel for protein export from *E. coli*: Reversible bridging of an inner-membrane translocase to an outer membrane exit pore. *EMBO J* 17:6487–6496.
17. Yamamoto K, et al. (2016) Substrate-dependent dynamics of the multidrug efflux transporter AcrB of *Escherichia coli*. *Sci Rep* 6:21909.
18. Elf J, Li G-W, Xie XS (2007) Probing transcription factor dynamics at the single-molecule level in a living cell. *Science* 316:1191–1194.
19. Chen T-Y, et al. (2015) Concentration- and chromosome-organization-dependent regulator unbinding from DNA for transcription regulation in living cells. *Nat Commun* 6:7445.
20. Outten FW, Huffman DL, Hale JA, O'Halloran TV (2001) The independent *cue* and *cus* systems confer copper tolerance during aerobic and anaerobic growth in *Escherichia coli*. *J Biol Chem* 276:30670–30677.
21. Long F, et al. (2010) Crystal structures of the CusA efflux pump suggest methionine-mediated metal transport. *Nature* 467:484–488.
22. Bagai I, Liu W, Rensing C, Blackburn NJ, McEvoy MM (2007) Substrate-linked conformational change in the periplasmic component of a Cu(I)/Ag(I) efflux system. *J Biol Chem* 282:35695–35702.
23. Kulathila R, Kulathila R, Indic M, van den Berg B (2011) Crystal structure of *Escherichia coli* CusC, the outer membrane component of a heavy metal efflux pump. *PLoS One* 6: e15610.
24. Su CC, et al. (2011) Crystal structure of the CusBA heavy-metal efflux complex of *Escherichia coli*. *Nature* 470:558–562.
25. Su CC, et al. (2009) Crystal structure of the membrane fusion protein CusB from *Escherichia coli*. *J Mol Biol* 393:342–355.
26. Zhang M, et al. (2012) Rational design of true monomeric and bright photoactivatable fluorescent proteins. *Nat Methods* 9:727–729.
27. McKinney SA, Murphy CS, Hazelwood KL, Davidson MW, Looger LL (2009) A bright and photostable photoconvertible fluorescent protein. *Nat Methods* 6:131–133.
28. Dammeyer T, Tinnefeld P (2012) Engineered fluorescent proteins illuminate the bacterial periplasm. *Comput Struct Biotechnol J* 3:e201210013.
29. Betzig E, et al. (2006) Imaging intracellular fluorescent proteins at nanometer resolution. *Science* 313:1642–1645.
30. Rust MJ, Bates M, Zhuang X (2006) Sub-diffraction-limit imaging by stochastic optical reconstruction microscopy (STORM). *Nat Methods* 3:793–795.
31. Hess ST, Girirajan TPK, Mason MD (2006) Ultra-high resolution imaging by fluorescence photoactivation localization microscopy. *Biophys J* 91:4258–4272.
32. Oswald F, Bank ELM, Bollen YJM, Peterman EJG (2014) Imaging and quantification of trans-membrane protein diffusion in living bacteria. *Phys Chem Chem Phys* 16: 12625–12634.
33. Chen T-Y, et al. (2015) Quantifying multistate cytoplasmic molecular diffusion in bacterial cells via inverse transform of confined displacement distribution. *J Phys Chem B* 119:14451–14459.
34. Kumar M, Mommer MS, Sourjik V (2010) Mobility of cytoplasmic, membrane, and DNA-binding proteins in *Escherichia coli*. *Biophys J* 98:552–559.
35. Nenninger A, et al. (2014) Independent mobility of proteins and lipids in the plasma membrane of *Escherichia coli*. *Mol Microbiol* 92:1142–1153.
36. Oh D, Yu Y, Lee H, Wanner BL, Ritchie K (2014) Dynamics of the serine chemoreceptor in the *Escherichia coli* inner membrane: A high-speed single-molecule tracking study. *Biophys J* 106:145–153.
37. Gambin Y, et al. (2006) Lateral mobility of proteins in liquid membranes revisited. *Proc Natl Acad Sci USA* 103:2098–2102.
38. Thiem S, Kentner D, Sourjik V (2007) Positioning of chemosensory clusters in *E. coli* and its relation to cell division. *EMBO J* 26:1615–1623.
39. Tikhonova EB, Yamada Y, Zgurskaya HI (2011) Sequential mechanism of assembly of multidrug efflux pump AcrAB-TolC. *Chem Biol* 18:454–463.
40. Krishnamoorthy G, Tikhonova EB, Dhamdhere G, Zgurskaya HI (2013) On the role of TolC in multidrug efflux: The function and assembly of AcrAB-TolC tolerate significant depletion of intracellular TolC protein. *Mol Microbiol* 87:982–997.
41. Bagai I, Rensing C, Blackburn NJ, McEvoy MM (2008) Direct metal transfer between periplasmic proteins identifies a bacterial copper chaperone. *Biochemistry* 47:11408–11414.
42. Mealman TD, et al. (2012) N-terminal region of CusB is sufficient for metal binding and metal transfer with the metallochaperone CusF. *Biochemistry* 51:6767–6775.
43. Mealman TD, et al. (2011) Interactions between CusF and CusB identified by NMR spectroscopy and chemical cross-linking coupled to mass spectrometry. *Biochemistry* 50:2559–2566.
44. Chacón KN, Mealman TD, McEvoy MM, Blackburn NJ (2014) Tracking metal ions through a Cu/Ag efflux pump assigns the functional roles of the periplasmic proteins. *Proc Natl Acad Sci USA* 111:15373–15378.
45. Yun B-Y, et al. (2010) Periplasmic domain of CusA in an *Escherichia coli* Cu^{+}/Ag^{+} transporter has metal binding sites. *J Microbiol* 48:829–835.
46. Kittleson JT, et al. (2006) Periplasmic metal-resistance protein CusF exhibits high affinity and specificity for both CuI and AgI. *Biochemistry* 45:11096–11102.
47. Loftin IR, Blackburn NJ, McEvoy MM (2009) Tryptophan Cu(I)-pi interaction fine-tunes the metal binding properties of the bacterial metallochaperone CusF. *J Biol Inorg Chem* 14:905–912.
48. Gudipaty SA, McEvoy MM (2014) The histidine kinase CusS senses silver ions through direct binding by its sensor domain. *Biochim Biophys Acta* 1844:1656–1661.
49. Lu S, Zgurskaya HI (2013) MacA, a periplasmic membrane fusion protein of the macrolide transporter MacAB-TolC, binds lipopolysaccharide core specifically and with high affinity. *J Bacteriol* 195:4865–4872.
50. Borges-Walmsley MI, et al. (2003) Identification of oligomerization and drug-binding domains of the membrane fusion protein EmrA. *J Biol Chem* 278:12903–12912.